Exp Fluids
DOI 10.1007/s00348-009-0624-7

RESEARCH ARTICLE

Time-resolved wake structure and kinematics of bat flight

Tatjana Y. Hubel · Nickolay I. Hristov · Sharon M. Swartz · Kenneth S. Breuer

Received: 20 June 2008 / Revised: 12 December 2008 / Accepted: 23 January 2009

Abstract We present synchronized time-resolved measurements of the wing kinematics and wake velocities for a medium sized bat, *Cynopterus brachyotis*, flying at low-medium speed in a closed-return wind tunnel. Measurements of the motion of the body and wing joints, as well as the resultant wake velocities in the Trefftz plane are recorded at 200 Hz (approximately 28–31 measurements per wing beat). Circulation profiles are found to be quite repeatable although variations in the flight profile are visible in the wake vortex structures. The circulation has almost constant strength over the middle half of the wing beat (defined according the vertical motion of the wrist, beginning with the downstroke). A strong streamwise vortex is observed to be shed from the wingtip, growing in strength during the downstroke, and persisting during much of the upstroke. At relatively low flight speeds (4.3 m/s), a closed vortex structure behind the bat is postulated.

1 Introduction

Humans have long been fascinated with the movement of animals through the air, and observations of nature's fliers' seemingly effortless defiance of gravity first inspired our dreams of taking to the air. In the centuries it took to achieve this goal, animal flight has not only aroused passion, but also served the more utilitarian function of inspiring design innovations, particularly during the earliest stages of aeronautic history. For example, observations of the wings of flying storks provided the first insight into the role of camber in the functional architecture of airfoils (Lilienthal 1889). Nonetheless, the early attempts to use flapping wings for propulsion were bound to fail, and consequently, research concerning flapping flight has been overshadowed by the study of fixed and rotating wings for almost 100 years, particularly outside of the communities of zoologists with particular interests in insects, birds, pterosaurs, or bats. Interest in bio-inspired flight among diverse groups of engineers has resurfaced in recent years, however, and both the desire to develop highly efficient and maneuverable MAVs, and the greatly improved capabilities of modern equipment to image animal motion at high speed and visualize complex fluid flows have returned attention to animal flight research. Over the last two decades, knowledge about insect and bird flight has advanced tremendously, and we have gained greatly improved understanding about a host of issues in animal flight, such as the scaling of flight performance and the importance of unsteady effects (Ellington 1999; Ellington et al. 1996; Hedenström et al. 2006; Sane 2003; Spedding et al. 2003).

Although bats are the only mammals that have achieved powered flight, their flight has received relatively little attention until recently (Hedenström et al. 2007; Muijres et al. 2008; Tian et al. 2006), in part due to their nocturnal lifestyle which has kept them, literally, out of the spotlight. These astonishingly accomplished flyers number over 1,200 species, making up about one quarter of the diversity of all extant mammals. Unlike birds and insects, which regularly employ many forms of terrestrial locomotion, the vast majority of bats rarely move more than a few meters by any form of locomotion other than flight. Their tremendous ecological diversity, however, encompasses most of the earth's habitats, and their dietary specializations include not only insects, but also fruit, flowers, pollen, fish

T. Y. Hubel (✉) · N. I. Hristov · S. M. Swartz · K. S. Breuer
Brown University, Providence, RI 02912, USA
e-mail: tatjana_hubel@brown.edu

Published online: 22 February 2009

and other small vertebrates, and even mammal and bird blood (Neuweiler 2000). They are able to land and roost on myriad substrates, can eat almost half of their body weight in a single night, and during pregnancy carry fetuses as large as a third of the mother's weight (Nowak 1994).

The flight of bats, much like that of birds has often been modeled to a first approximation as quasi-steady, with wings treated as rigid plates (Pennycuick 1968; Rayner 1979; Tobalske et al. 2003a). The assumption of steady flight was largely necessitated by the lack of analytical and experimental tools to analyze more complex flows, but this situation has changed considerably in the past few years. Similarly, the treatment of wings as rigid plates was initially one of simplicity, and has proved quite reasonable for some aspects of the flight of insects and even birds (Tobalske et al. 2003b). Bat wings are, however, anything but rigid, and are characterized by structural design that embodies a unique amount of flexibility (Swartz et al. 2006). In particular, bat wings possess more than two dozen joints, highly deforming bones, and anisotropic wing membrane skin with variable stiffness (Swartz et al. 1996). Even in level flight at constant speed, bat wings differ from those of birds and insects in their large and dynamically changing camber, and complex kinematics. As a consequence, aerodynamic models of bat flight that do not account for the dynamic aspects of the bat wing architecture can provide a starting point for understanding the mechanistic basis of bat flight, but are ultimately limited in explaining the ways that bats produce the aerodynamic forces required for flight. We can therefore expect that studies that account for the dynamic conformation of bat wings will substantially improve understanding of the aeromechanics of bat flight. Because of the distinctive anatomy of the bat wing, and the particular evolutionary history of bats, descendents of mammalian ancestors with highly complex and flexible locomotion, bats may represent the extreme among flying animals in this regard (Fig. 1).

In this paper, we describe aspects of the flight mechanics of a non-echolocating bat of intermediate body size, the Lesser dog-faced fruit bat, *Cynopterus brachyotis*. To better understand bat aerodynamics in the context of the time-varying three-dimensional structure and posture of the wing, we have simultaneously captured detailed wing kinematics and wake structure by using multiple camera high speed videography synchronized with time-resolved particle image velocimetry (PIV). Attempts to gain insight into the mechanistic basis of flight from PIV independent of wing kinematics will achieve limited success compared to analyses that link the development and evolution of wake structure to the dynamically changing shape of the wing. PIV is a powerful tool to enable researchers to better understand the aerodynamics of animal flight, but is most valuable when coupled directly to detailed kinematics, particularly for animals whose wings employ a large range of motion and dramatic modulations of three-dimensional conformation and stiffness.

The approach we use here, employing a 200 Hz PIV system, allows us to observe the details of wake development over multiple wing beat cycles, avoiding the necessity of building a composite picture of wake development by concatenating results obtained from multiple trials or wing beats at low sampling rates. We demonstrate that this coupling enables the exploration of relatively fine-scale variation in wing kinematics, wake structure, and kinematic/aerodynamic interrelationship. Understanding the significance of kinematics and aerodynamics at a fine-scale is critical to understanding flight variation within individuals and individual variation within-species for a given flight condition, such as level flight at constant speed. Also, importantly, the variation observed during other flight behaviors, such as changing speed, maneuvering, or changing altitude must be analyzed. Furthermore, the explicit coupling of kinematic and wake structure analysis can provide a fruitful framework for evaluating the possibility of aerodynamically distinctive flight gaits in bats.

As a crucial early step toward achieving the long-term goal of fully integrated analyses of complex kinematics and aerodynamics, our specific focus in this paper is time-resolved wake structure, and its spatial and temporal

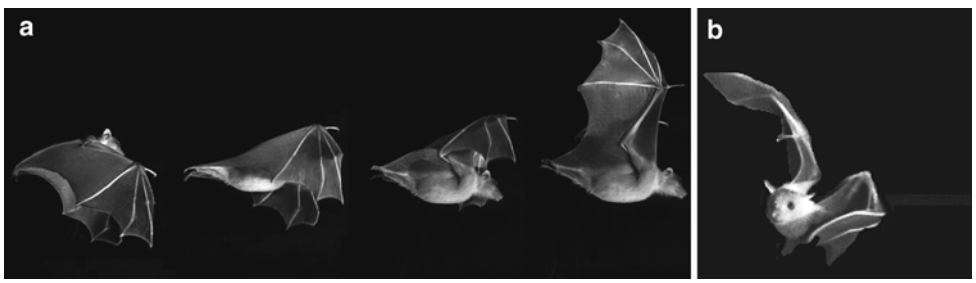

Fig. 1 Complex wing kinematics, shape change, and bending in bat flight. **a** *Cynopterus brachyotis*, the Lesser dog-faced fruit bat, in steady flight (Re = 27,000) in the Brown University wind tunnel, illustrating multiple stages in the upstroke. **b** *Cynopterus brachyotis* maneuvering in wind tunnel test section

relationships with the motions of the wing tip and wrist. Future reports will build on these fundamental relationships by providing a more comprehensive analysis of the joint motion, membrane dynamics, and their detailed connections with the wake flow structures.

2 Experimental methods

2.1 Bats

We trained Lesser dog-faced fruit bats, *Cynopterus brachyotis*, to fly in the low-speed wind tunnel in the Division of Engineering at Brown University. These captive-bred female bats, on loan from the Lubee Bat Conservancy (Gainsville, Florida) received a 15–20 min wind tunnel training two to four times a week over a period of 2 months prior to the experiments reported here.

2.2 Wind tunnel

The low speed wind tunnel we employed has a closed-circuit design and has a test section measuring 3.8 m in length, with a cross-section of 0.60 by 0.82 m (height × width). Although the free stream turbulence level of the tunnel is quite low (0.29% at 2.81 m/s), a fine-mesh net is placed at the upstream entrance to the test section to restrict the bats, and this results in a turbulence level of 0.5% at 2.8 m/s at the location of the PIV observation area. Antireflective glass plates on bottom, top, and portions of the side of the test section, and Plexiglas windows on the walls allow almost unhindered visibility (Fig. 2). The bats are introduced to the flow by a member of the research team at a station approximately 0.5 m downstream of the measurement section. They fly into the oncoming air stream, moving slowly up the test section towards the settling chamber. Having flown sufficiently upstream and beyond the measurement volume, they are "retrieved" from the test section by a second research team member. The test section is sufficiently long (3.8 m) such that the measurement area is far from the points of introduction and retrieval, and during measurements, Plexiglass doors were closed to prevent the generation of any additional turbulence in the test section. We define a right-handed coordinate system with positive x defined in the direction of the wind (negative in the flight direction of the bat). The z-coordinate is positive in the vertical upward direction, and y is positive from center of the bat towards the tip of the right wing. Our results are usually presented in a bat-centered coordinate system, but depending on the specific goal of the analysis, sometimes in a combination of wind tunnel and bat-centered coordinate systems, with y and z in bat-centered coordinate system, with the origin located between the shoulder blades (along the midline of the back, roughly 1.5 cm posterior to the neck) and with the origin of the x-axis fixed at the plane where PIV measurements were acquired.

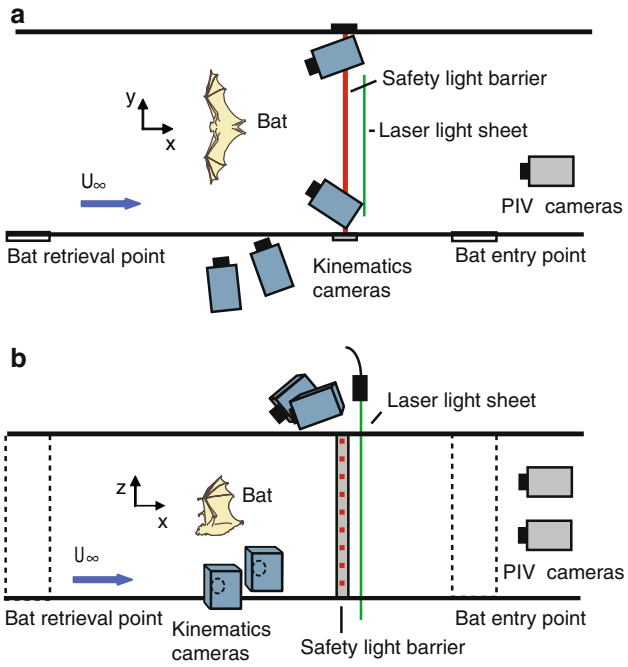

Fig. 2 Top (**a**) and Side (**b**) schematic views of the experimental setup in the wind tunnel for measurements in the transverse plane, perpendicular to the flow stream (Trefftz plane). The kinematics cameras are positioned above and beside the test section, out of the air stream, while the PIV cameras are in the test section, oriented perpendicular to the flow stream. The safety light-curtain is positioned 5 cm upstream of the laser light sheet. The locations of the introduction and retrieval of the animal are windows on the side of the test section

2.3 PIV

To obtain the wake velocity components, we performed time-resolved PIV using a 200 Hz double-pulse Nd:YAG laser (Litron LPY 703-200) to illuminate the observation area (pulse duration 6 ns, energy 60 mJ). The wind tunnel was seeded with di-ethyl-hexyl-sebacate (DEHS) using a custom built Laskin-type nozzle fog generator.

Two high-resolution CMOS cameras (Photron 1,024 PCI, resolution 1,024 × 1,024 pixels, lens 85 mm, f/1.4) captured the motion of the DEHS particles in the observation area. The two PIV cameras were located at the downstream end of the test section, and positioned perpendicular to the flow stream so as to capture the wake structure in the Trefftz (y–z) plane. The two cameras imaged overlapping but separate fields of view to maximize the size of the observation area. A single calibration

plate and the coordinate system origin were visible in both cameras, with an overlap of approximately 0.05 m, and the resulting image size was 0.23 m × 0.41 m. This field of view was sufficient to image the complete wake of the right wing; in our analyses, we mirrored this wake structure to visualize the entire wake for ease of viewing, using the assumption that left and right wing motions differ little in straight, steady flight.

We recorded PIV data using a buffer loop function to record the data in an endless loop triggered by an END signal (DaVis 7.13 software, LaVision). The calibration parameters are achieved by using the pinhole calibration, and the two camera images stitched together within the software. Vector fields were calculated using cross-correlation with multi-pass iterations with decreasing size (128 × 128, 2 iterations to 64 × 64, 2 iterations, 50% overlap) resulting in a 32 × 56 vector field. Vectors with peak ratio $Q < 1.2$ and variations to the average neighborhood >1.5 × r.m.s. of neighbor vectors were replaced via interpolation (average replacement 1.7%, average Q-value 2.96) and a simple 3 × 3 smoothing filter was applied. The vector field was exported and subsequently processed in Matlab®.

Circulation (Γ) was obtained by integration of the vorticity (ω_x) over the area to the right of the body marker. The measured velocity and vorticity fields are typically noisy and for this reason, there are several viable methods for estimating the circulation. One method is to integrate only the vorticity that rises above an arbitrary threshold, and subsequently to add back an analytical estimate for the neglected vorticity (Spedding et al. 2003). Another method is to calculate the swirl from the velocity field (i.e. the rotational part of the local two-dimensional rate-of-strain tensor) and to use this as a mask for the circulation calculation (thus filtering out vorticity due to local shear). Our approach was to integrate the entire measurement area to the right of the body, assuming that positive and negative vorticity due to turbulence will cancel out, leaving only the coherent circulation generated by the bat. The resulting average circulation generated over one wing beat cycle can differ up to 30% depending on the chosen method, however the primary vortex structure and its temporal development (if not the absolute value) was found to be very consistent between different methods.

The circulation was normalized by average wing chord (c) and the true flight velocity, such that $\gamma = \Gamma/(U_t)c$. The true flight speed (U_t) combines the wind speed with any additional flight speed of the bat (U_b). Since the bat was usually moving up the test section, flying towards the front screen (in the negative x-direction in the wind tunnel coordinate system), the velocity of the bat was actually negative and the true flight speed is $U_t = U_\infty - U_b$. We calculated local circulation maxima and minima and defined the wing beat cycle as the period between two minima.

The flapping frequency based on the wake measurements (f_{PIV}) was calculated according to the period. However, due to the movement of the bat in the test section, the wake frequency can be different from the true flapping frequency due to a Doppler shift:

$$f_t = \frac{U_t}{U_\infty} f_{PIV}$$

where f_t is the true flapping frequency. We have also assumed that the wake vortex structure travels at the free stream velocity. The actual flapping frequency was also extracted directly from the kinematics (f_K) and compared with the wake-based flapping frequency (f_{PIV}) and the corrected true flapping frequency (f_t). Subsequently, the true flapping frequency (f_t) and true flight speed (U_t) are used to calculate Reynolds number ($Re = (U_t c)/\nu$, reduced frequency ($k = (\pi f_t c)/U_t$) and Strouhal number ($Sr = (f_t A)/U_t$) (ν is the kinematic viscosity, A is the wingtip excursion, the vertical distance traveled by the tip of the wing during the flapping stroke).

Small variations in the flapping frequency of consecutive wing beat cycles led to a variable number of computed values of the velocity field and circulation during each cycle (approximately 28–31), and to address this, we partitioned each wing beat cycle into 35 segments and used interpolation to compute the circulation for 35 time increments per wing beat cycle. We estimated a moving average over three values, and then computed the mean and standard deviation of the circulation over six consecutive wing beat cycles. Six cycles were chosen because this was the maximum number of consecutive wing beat cycles available for all trials.

To visualize the development of the wake structure over time, we first convert time to streamwise distance (assuming that the wake structures advect with the freestream velocity) and plot an isosurface of the swirl (Adrian et al. 2000), therefore taking only the rotational part of the vorticity from PIV measurements in the Trefftz (y–z, or transverse) plane into account. While visualization of the vorticity field requires additional smoothing and a high threshold (±50% of maximum vorticity value) to enable a clear visualization of the main vortex, the swirl is effectively seen using a very low threshold (we use isosurfaces of 2.5% of the maximum swirl value), and requires no additional smoothing. This also allows us to show the development of small, but coherent, vortex structures that appear during the wing beat cycle, but are difficult to see using vorticity visualization. Swirl does not differentiate between counter- and clockwise rotating vortices and so the vorticity field was used to determine the local rotational direction, and a color was assigned, based on the circulation at that particular time.

2.4 Kinematics

Kinematic data were recorded using four cameras (Photron 1,024 PCI, resolution 1,024 × 1,024 pixels, 200 fps) positioned above and alongside the test section (Fig. 2). The cameras were synchronized with the PIV recordings by using a laser flash lamp sync signal to trigger a digital delay-pulse generator (Model 555 Berkeley Nucleonics Corporation). Kinematic and PIV cameras shared a single origin and coordinate system; calibration was achieved with the direct linear transformation (DLT) method (Abdel-Aziz and Karara 1971) following videographic recording of a calibration plate mounted on a linear traverse, moved through the control volume by successive displacements of 0.1 m. Seventeen white circles marked the joints and other important anatomical positions on the dorsal surface of the bat (Fig. 3). The kinematic measurements were sub-sampled by a factor of ten using a spline interpolation to fill gaps in the data due to obstruction of markers. This method ensured the accuracy of the correlation between the PIV and kinematic measurements, as well as during the correction of the PIV data to account for the Doppler shift described above.

2.5 Light

To minimize light pollution, the PIV cameras were equipped with 532 nm band-pass filters transmitting light in the range of 511–548 nm. Narrower filters darkened videographic images significantly and were not usable. The kinematics volume was illuminated by three Xenon strobe lights (Nova-Strobe dax, Monarch Instrument) operating at 200 Hz, and synchronized with the kinematics cameras. The strobe lights emit short (10–25 μs) intense light pulses which provide sufficient illumination for the kinematic recordings, eliminate motion-induced blurring while maintaining a low average light level, which is preferred by the nocturnal bats. By pointing the strobes away from the PIV cameras, we kept reflections to a minimum. This approach also allows us to interlace the PIV lasers with the strobe lights, thus further reducing light pollution during image capture for PIV. However, this was not found to be necessary and was not used in the experiments reported here.

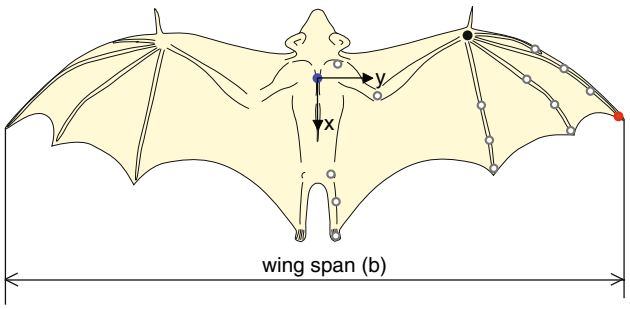

Fig. 3 Positions of kinematics markers on the dorsal surface of the bat. Body (*blue circle*) and wrist (*black circle*) and wing tip (*red circle*) position of the bat, *x* and *y* indicate the body fixed coordinate system

2.6 Light curtain

The intense energy in the PIV laser light sheet is capable of injuring bats in several ways, particularly their eyes, so the operation of the PIV system was gated by a laser light safety curtain, positioned 0.05 m upstream of the laser light sheet. The safety curtain consisted of an array of 21 low-power red diode lasers spanning the entire test section, each aimed at a complementary photo-diode. After the bat was released and had safely advanced upstream of the light curtain, the system was activated. If the bat moved downstream for any reason, it would interrupt one of the safety beams, at which point the laser system automatically shut down.

3 Results and discussion

We present results collected in four trials of three bats. The original data collection included measurements using three individuals flying at freestream velocities ranging from 3.5 to 5.5 m/s. Measurements such as these, using un-tethered live animals, are difficult, and for this reason, the present manuscript only reports on four trials obtained using three bats (Table 1).

Wing beat kinematics for bat flight are extremely complex (Riskin et al. 2008) and beyond the scope of this paper. Because the wing changes shape continuously as it flaps, it cannot be viewed as a flapping plate, or even as a flapping plate with one or two simple hinges. Many of the joints of the handwing are extended during the downstroke until the lower reversal point, at which point they begin to flex, and the wingtip moves closer to the body in horizontal direction. At the same time, early in the upstroke, the wingtip moves simultaneously upwards and outwards. At the end of the upstroke, the wing has adopted a rather extended posture. Moreover, the motion of the wingtip is not primarily vertical with respect to either gravity or the animal's body. The wings sweep forward as they move downward, increasing the relative forward velocity during downstroke, and decreasing angle of attack and backwards sweep during upstroke.

A sample trace of the vertical motion of the wrist and wingtip with respect to the body (Fig. 4), illustrates the phase and position difference between the wingtip and the wrist. Although the wingtip motion has larger amplitude,

Table 1 Physical characteristics of the three bats

Individual	Mass (kg)	Average chord (m)	Maximum span (m)	Maximum wing area (m^2)	Aspect ratio (-)	Wing loading (N/m^2)
Bat 1	0.033	0.061	0.406	0.025	6.59	13.20
Bat 2	0.029	0.059	0.376	0.022	6.43	13.18
Bat 3	0.030	0.058	0.399	0.023	6.92	13.04

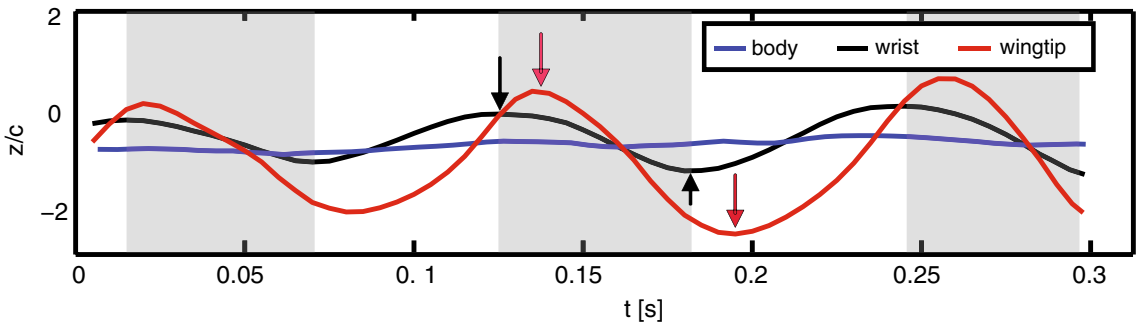

Fig. 4 Lateral view of the trace of body, wrist and wingtip motion. The *shaded areas* represent the downstroke (as defined by the wrist motion). The body motion is usually quite steady, although does show some periodic variation associated with the wing beat cycle. The *arrows* marking the beginning and end of the downstroke of the wrist (*black*) and wing tip (*red*) and reveal the fact that the phase of the wingtip motion lags that of the wrist

we choose to define the upstroke and downstroke according the wrist motion because it has a more purely sinusoidal motion, and the movement of the wrist is more directly controlled by the primary flight musculature.

Many flights are highly regular, with stereotyped kinematic patterning and hence aerodynamics. However, some trials display substantial variation in the observed patterns of circulation from one wing beat cycle to the next. For example, in one flight (Fig. 5), the wing beat cycles early in the flight are very consistent, with little variation in either flapping frequency (f_{PIV} = 7.7 Hz ± 0.4) or mean normalized circulation (0.132 ± 0.015); later in the same flight, both wing beat frequency and normalized circulation decrease temporarily as the subject slowed, then accelerated. Such variation among wingbeats within a single flight sequence of a single individual highlights the benefits of high frequency PIV experiments. Using a low-frequency PIV system in which the laser repetition rate is low relative to wing beat frequency, it is necessary to piece together records from multiple wing beats to create a single composite wing beat cycle, and such inconsistencies and variation among wing beats are more likely to lead to errors than to new insights. Similar difficulties might also arise from PIV without synchronized and detailed kinematic measurements.

The bat flies upstream in the wind tunnel, away from the laser light sheet, and therefore the distance between the vortex generation and the measurement plane increases (up to 2 m) as the measurement sequence progresses. If there

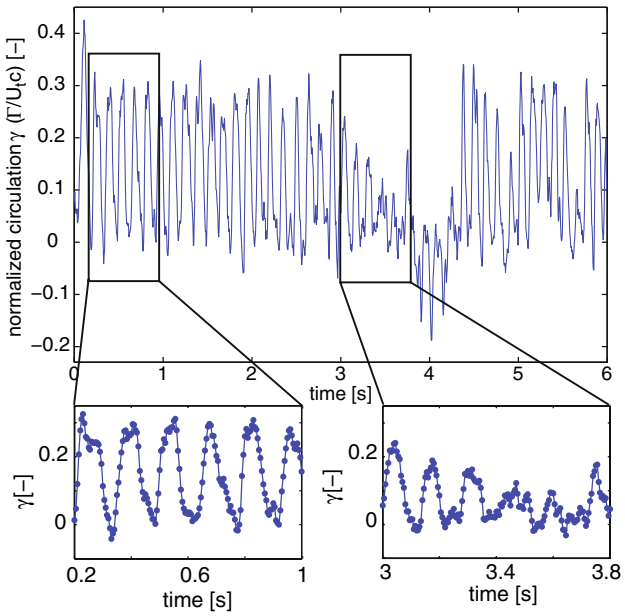

Fig. 5 Normalized circulation versus time at Re = 20,000, k = 0.28 (bat 2) derived from the wake PIV measurements. For this particular trial, PIV data was obtained for over 6-s and approx. 45 wing beats. At the beginning of the trial there is a good uniformity in the flapping frequency, amplitude and shape of the circulation cycle. However, differences are observed in the middle of the record, corresponding to observed deceleration and manoeuvring by the bat

were a significant influence of the vortex convection time, one would expect to see this reflected in a change in the measured vortex structure over the duration of the sequence.

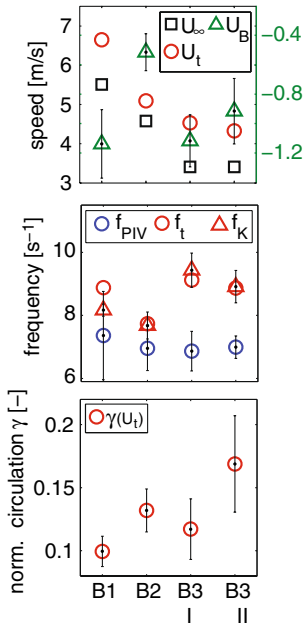

Fig. 6 Flight speed, flapping frequency and circulation from four trials with three individuals. *Top frame*: wind speed (U_∞), bat speed relative to the wind speed and in opposite direction and therefore negative (U_B) and the true flight speed ($U_t = U_\infty - U_B$); *Middle frame*: flapping frequency derived from (1) PIV (f_{PIV}) (2) PIV, adjusted for Doppler shift (f_t), and (3) derived from kinematics (f_K); Lower frame: normalized circulation (based on the true flight speed) (γ)

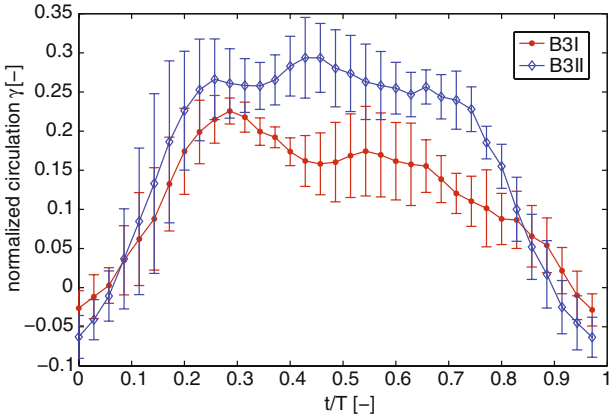

Fig. 7 Development of the normalized circulation over one wing beat cycle, averaged over six wing beats. Two trials are shown from the same individual flying at $Re = 17{,}500$ and 16,700 with $k = 0.38$ in both cases. The variation in the circulation appears to be related changes in altitude during the measurement window

However, although small flow structures that are visible in the first couple of wing beat cycles do seem to disappear with time (Fig. 10), the overall structure and amplitude of the circulation over the wing beat cycles (Fig. 5) and the average circulation do not decrease in any significant manner, and we therefore assume that dissipation and flow unsteadiness, at least of the large-scale structures, are not of primary importance and can be neglected.

The circulation and flapping frequency was averaged over six wing beat cycles for four trials of three different bats (Fig. 6). The frequency of the circulation signature measured in the wake (f_{PIV}) varies very little, typically around 7 Hz. However, U_B, the motion of the bat relative to the test section, was typically between -0.5 and -1.1 m/s (negative due to the bats upstream motion), and when wingbeat frequency is corrected for the Doppler shift due to this relative motion, the wake frequency closely matches the frequency measured directly from the kinematic record. Reynolds number, reduced frequency and Strouhal number vary among the bats, but are consistent between the two trials of the same bat (Table 2).

Although it is not surprising that the normalized circulation varies from bat to bat, in part because no two bats possess identical body mass, there is also a marked difference between consecutive trials of the same individual (bat 3) flying at the same reduced frequency (Fig. 6). Figure 7 presents a view into the development of the circulation over the wingbeat cycle for this case and emphasizes the difference, with trial no. 2 exhibiting a consistently higher circulation than trial no. 1 over the central core of the wingbeat, $t/T = 0.2$–0.8. Examination of the kinematics results reveals that the two trials are characterized by different vertical histories, with the bat in trial no. 1 moving downwards 13% of the horizontal travel distance and moving upwards 8% in trial no. 2. It is important to account for these changes in altitude in detailed aerodynamic analyses, and we will explore these specifics in more detail in future work.

The average circulation is only about one half the value that one would expect to see based on weight support at the observed flight speed. This is, of course, a serious concern, and we have explored the issue quite thoroughly. We are confident that the measurements presented are not dependant on PIV acquisition or processing parameters (e.g. time between laser pulses, interrogation window area, overlap, filtering, etc.). We speculate that two issues are primarily responsible for the discrepancy. Firstly, it is possible that a portion of the tip vortex structure is destroyed by background turbulence and other unsteady vortex structures shed by the bat. Secondly, it is possible that a significant fraction

Table 2 Reynolds number (Re), reduced frequency (k) and Strouhal number (Sr) for three different bats and four trials based on the true flapping frequency and flight speed

	Bat 1	Bat 2	Bat 3 trial I	Bat 3 trial II
U_∞ (m/s)	5.51	4.58	3.41	3.41
Re	27,000	20,000	17,500	16,700
k	0.24	0.28	0.38	0.38
Sr	0.25	0.28	0.42	0.41

of the vortex sheet shed by the wing may be lost due to diffusion before it is gathered up into the primary tip vortex. This idea is supported by recent experiments (Gerontakos and Lee 2006) conducted using both swept and rectangular wings at $Re = 181{,}000$, which found similarly small fractions of the total shed circulation present in the tip vortex structure. We also explored this by measuring the tip vortex behind a rigid rectangular wing at several Reynolds numbers, including those comparable to the bats' flight conditions (Table 2). We found that the measured circulation was only about 50% of that predicted by thin airfoil theory, and measured directly using a load cell, thus supporting the idea that, while the vortex structure accurately reflects the nature of the lifting body, at these low Reynolds numbers, the tip vortex might not capture the total circulation associated with the bound vorticity on the lifting surface. This is an ongoing investigation.

In *C. brachyotis* at moderate flight speed, circulation is generated continually during a large part of the downstroke and part of the upstroke (Fig. 7). At the beginning of the downstroke, the streamwise vorticity field in the wake shows no presence of a distinct vortex structure (Fig. 8a). At the end of the first third of the downstroke the wake measurements indicate the development of a single streamwise vortex structure that starts at a point 1.5 half-spans above the center-plane. The structure continues to gain strength while moving downwards and outwards (Fig. 8b), reaching maximum strength 1.5 half-spans below the center-plane at the end of the downstroke. This maximum strength remains approximately constant during transition between downstroke and upstroke, although the vortex moves upward and inboard as the upstroke begins (Fig. 8c). The vortex structure remains during most parts of the upstroke, and begins to weaken during the middle of the upstroke. At the end of the upstroke and beginning of the downstroke, little or no circulation is generated. The development of the wingtip vortices shows some similarities to the pattern identified in previous measurements made at lower temporal resolution (Tian et al. 2006), but

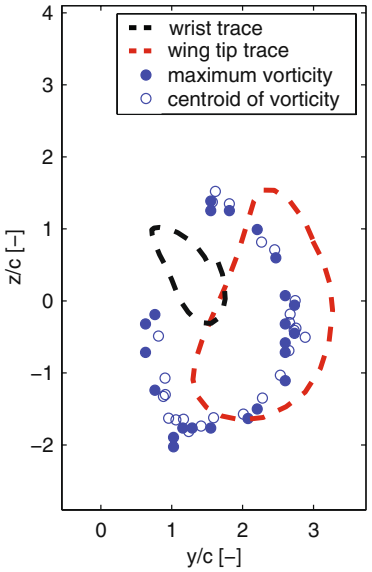

Fig. 9 Correlation between the wrist and wing tip locations and the tip vortex location, calculated from both the maximum vorticity and the centroid of vorticity ($Re = 16{,}700$, $k = 0.38$). The vortex core tracks the wing tip motion very closely, lying inboard by approximately $0.5c$, consistent with the location of the tip vortex shed from stationary fixed wings (Betz 1932; Devenport et al. 1996)

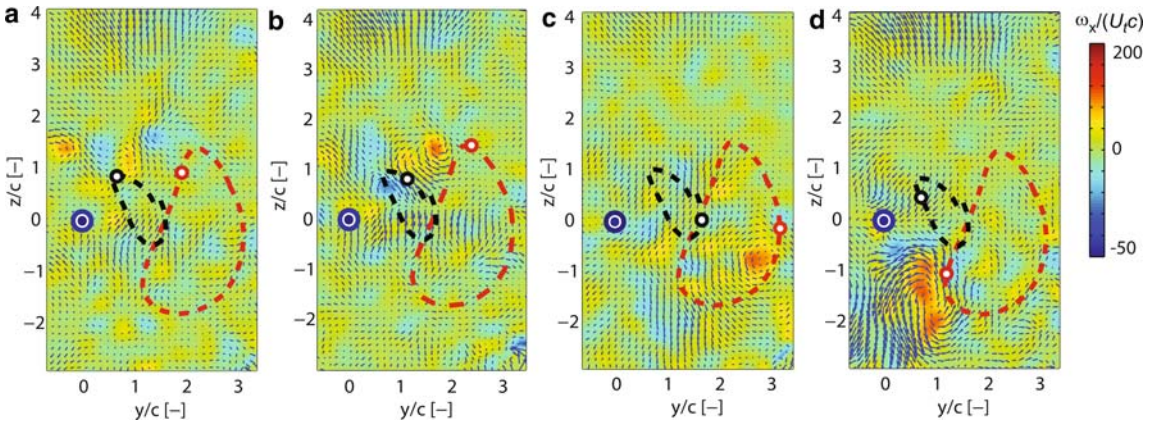

Fig. 8 Vector velocity field and streamwise vorticity at $Re = 16{,}700$, $k = 0.38$ in the plane perpendicular to the flow stream. The vorticity is shown behind the right wing of the bat in the coordinate system, where z and y coordinates are body-centered and normalized by the average wing chord. No distinct vortex structure at the beginning of the downstroke (**a**). Formation of the tip vortex during the first third of the downstroke (**b**) gaining strength while moving downwards and outwards during the second third of the downstroke (**c**). The tip vortex gains maximum strength at the end of the downstroke, keeping it while moving in and upward (**d**) and stays present till almost the end of the upstroke—Body (*large blue double circle*) and wrist (*black circle*) and wing tip (*red circle*) position of the bat are computed from kinematics. The motion of the wrist and wingtip over one wing beat cycle, projected on the y–z plane, is indicated by the *dashed black and red line*, showing the phase difference between wrist and tip position

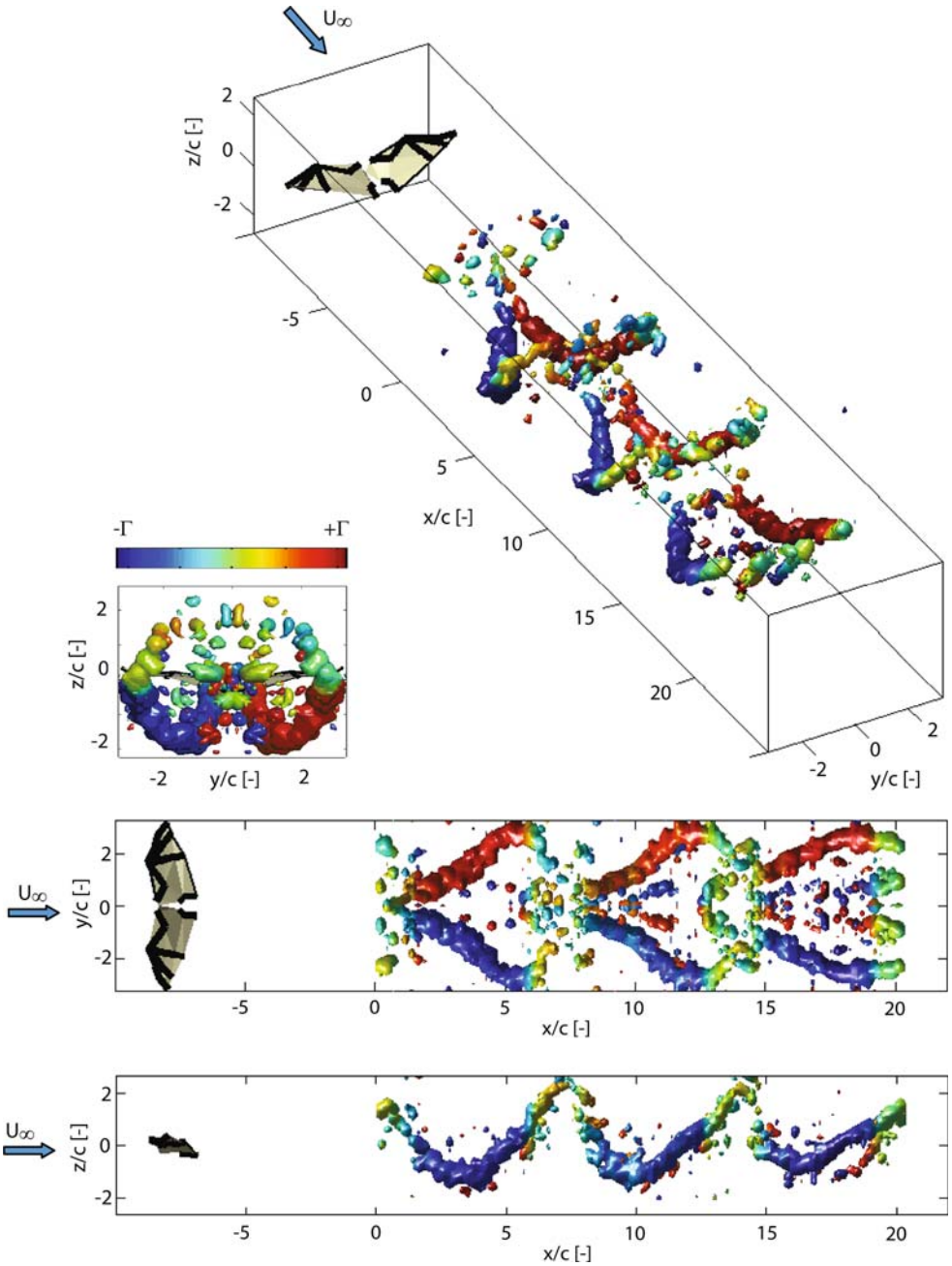

Fig. 10 Reconstruction of the wake of *C. brachyotis* flying at $Re = 16{,}700$, $k = 0.38$. Isosurfaces of the streamwise swirl from the right wing tip vortex are shown (and mirrored on the left side for ease of viewing). The y and z axis are as defined in Fig. 8. The origin of the x-axis is the position of the laser light sheet. The streamwise coordinate is derived from the time series using $x(t) = (U_\infty^2/U_t)(t_0 - t)$, where t_0 is the duration of the measurement sequence. At every instant in time, each vortex structure is assigned a rotational direction using the sign of the local vorticity, and is colored based on the magnitude of the total circulation at that time. This accurately reflects the changes in the circulation over the wing beat cycle, but does not allow for a quantitative comparison between clockwise and counter-clockwise vortices at any given time

also distinct differences, especially in terms of the correlation between kinematics and wake structure. These differences likely derive from the difficulties associated with the low-frequency of data acquisition in the previous work, and emphasize the importance of the simultaneous time-resolved measurements of wake and motion.

There are at least two ways to identify the center of the tip vortex: as the location of maximum vorticity in the observation area, or as the location of the centroid of the vortex, based on a threshold of 20 s^{-1} to avoid identifying maxima at times were no defined tip vortex was present. The spatial geometry of the tip vortex motion does not depend on the method (Fig. 9), and in both cases the vortex core tracks the wing motion very closely, lying inboard by approximately $0.5c$. This is consistent with predicted location of the tip vortex shed from a stationary fixed wing (Betz 1932; Devenport et al. 1996).

The observation of the streamwise vorticity, as well as the calculated circulation, suggests a wake structure of closed vortex loops similar to that observed during the slow flight of some birds (Spedding 1986; Spedding et al. 1984), rather than a constant circulation wake, as postulated for birds in cruising flight (Spedding 1987; Spedding et al. 2003). A ring vortex wake structure is also consistent with

aerodynamic interpretations based on calculations derived from kinematic modeling of displacements of the center of mass of the body plus flapping wings (Iriarte-Diaz et al. 2009a). However, large parts of the upstroke are aerodynamically active and contribute a considerable portion of the overall wing beat circulation. The aerodynamically inactive phase is limited to the portion over the wingbeat cycle close to the upper reversal point. The streamwise swirl topology (Fig. 10) demonstrates a characteristic "wishbone" structure, but shows a more complex vortex structure than that observed in bird flight; this pattern is consistent with observations made from flights of a smaller, nectar-feeding bat, *Glossophaga soricina* (Hedenstrom et al. 2007). Our reconstruction reveals a secondary vortex structure close to the body, similar to one observed for *G. soricina* in medium and slow flight. However, in the present case, the secondary structure is considerably weaker. While the one visualized for *G. soricina* was reported to have approximately 50% of the strength of the tip vortex, for *C. brachyotis,* maximum secondary vortex strength is only 8% of the maximum tip vorticity present in the wing beat cycle. The vortex structure close to the body rotates in the opposite direction to that of the tip vortex, and is present over the whole wing beat cycle. Due to its low amplitude, it can only be visualized from wing beat cycles in which the bat flew very close to the measurement plane. When the bat is further upstream, the weak structure has probably decayed by the time it advects to the PIV measurement plane, and thus it cannot be detected. The three displayed wing beats indicate a very repeatable wake structure during the consecutive wing beat cycles. Although the tip vortex was present during most of the upstroke, we have a more frequent occurence of weak vortices, both positive and negative, at the end of the upstroke and beginning of the downstroke.

These likely are shed from the body and the highly folded wing, but thus far no clear structure has been identified in the measurements (Fig. 8a) and additional data from further investigations will be required to fully resolve this issue. The slow formation of the streamwise vortex during the downstroke and its rather abrupt disappearance at the end of the upstroke suggests that slow flight in these bats is characterized by a number of relatively weak starting vortices, and in contrast, a single, strong stopping vortex at the end of the wing beat cycle.

4 Concluding remarks

Although these results do not provide a complete description of the complexity of mechanics of flight of even a single species of bat, the demonstration of high-resolution kinematics synchronized with time-resolved wake velocity measurements represents an important advance in experimental capabilities for the study of animal flight, and greatly advance our understanding of bat aeromechanics. Unlike previous methods which have relied on the assembly of a "typical" wake structures to form a composite view, the current methods allow for the full variability of the wake structure to be directly assessed and indentified with changes in wing and body kinematics. Wingbeat to wingbeat, flight-to-flight, and individual variability are increasingly recognized as important issues in natural animal flight, and are only recently being quantified (Iriarte-Diaz et al. 2009b) The techniques we employ here will provide the necessary framework to explore the aerodynamic aspect of variability in animal flight in significantly more detail than has previously been possible.

Despite the limited nature of the current data set, we can draw some important conclusions. A closed loop vortex structure is dominant at these relatively slow forward flight speeds, and there is evidence for additional small vortex structures shed from other appendages. In the future, a larger data set will allow us to make more general statements about the vortex structure at different flight speeds, and measurements in the parasaggital (x–z) plane as well as three-component PIV will provide more detail on these structures. It will also be possible to make direct comparisons between experimental, PIV measured wake structures and numerical simulations based on kinematics of the same bat species (Willis et al. 2007) Continuing advances in experimental approaches thus promise greatly improved understanding of the complex mechanisms of the flapping flight of bats in the coming years.

Acknowledgments We thank A. Song, R. Waldman and D. Riskin for helpful discussions, and A. Sullivan, L. Macayeal and A. Robb for handling and training of animals and their help with data collection. We are very thankful for the support provided by D. Riskin regarding kinematic analysis and data flow issues. We also thank R. Waldman for the construction of the safety light barrier. We thank the Lubee Bat Conservancy, especially A. Walsh, for the long term access to the bats. This work was supported by the Air Force Office of Scientific Research, monitored by Drs. Rhett Jeffries, John Schmisser and Willard Larkin, and the National Science Foundation. All experiments were conducted with the authorization of the Institutional Animal Care and Use Committees of Brown University, the Lubee Bat Conservancy and the Division of Biomedical Research and Regulatory Compliance of the Office of the Surgeon General of the United States Air Force.

References

Abdel-Aziz YI, Karara HM (1971) Direct linear transformation from comparator coordinates into object space coordinates in close-range photogrammetry. In: Proceedings of the symposium on close-range photogrammetry, American Society of Photogrammetry, Falls Church, pp 1–18

Adrian RJ, Christensen KT, Liu ZC (2000) Analysis and interpretation of instantaneous turbulent velocity fields. Exp Fluids 29:275–290

Betz A (1932) Verhalten von Wirbelsystemen. Zeitschrift fur angewandte Mathematikund Mechanik 12:164–174 (Also published as NACA TM 713)

Devenport WJ, Rife MC, Liapis SI, Follin GJ (1996) The structure and development of a wing-tip vortex. J Fluid Mech 312:67–106

Ellington CP (1999) The novel aerodynamics of insect flight: applications to micro-air vehicles. J Exp Biol 202:3439–3448

Ellington CP, van den Berg C, Willmott AP, Thomas ALR (1996) Leading-edge vortices in insect flight. Nature 384:626–630

Gerontakos P, Lee T (2006) Near-field tip vortex behind a swept wing model. Exp Fluids 40:141–155

Hedenström A, Johansson LC, Wolf M, von Busse R, Winter Y, Spedding GR (2007) Bat flight generates complex aerodynamic tracks. Science 316:894–897

Hedenström A, Rosén M, Spedding GR (2006) Vortex wakes generated by robins *Erithacus rubecula* during free flight in a wind tunnel. J Royal Soc Interface 3:263–276

Iriarte-Diaz J, Riskin DK, Willis DJ, Breuer KS, Swartz SM (2009a) No net thrust on the upstroke: whole-body kinematics of a fruit bat reveal the influence of wing inertia on body accelerations (in review)

Iriarte-Diaz J, Riskin DK, Swartz SM (2009b) Modulation of wingbeat kinematics with flight speed in the fruit bat *Cynopterus brachyotis* (in prep.)

Lilienthal O (1889) Der Vogelflug als Grundlage der. Fliegekunst Leipzig: Gaertuer

Muijres FT, Johansson LC, Barfield R, Wolf M, Spedding GR, Hedenstrom A (2008) Leading-edge vortex improves lift in slow-flying bats. Science 319:1250–1253

Neuweiler G (2000) The biology of bats. Oxford University Press, Oxford

Nowak RN (1994) Walker's bats of the world. Johns Hopkins University Press, Baltimore

Pennycuick CJ (1968) Power requirements for horizontal flight in the pigeon Columba Livia. J Exp Biol 49:527–555

Rayner JMV (1979) A vortex theory of animal flight. Part 2: the forward flight of birds. J Fluid Mech 91:731–763

Riskin DK, Willis DJ, Iriarte-Díaz J, Hedrick TL, Kostandov M, Chen J, Laidlaw DH, Breuer KS, Swartz SM (2008) Quantifying the complexity of bat wing kinematics. J Theor Biol 254:604–615

Sane SP (2003) The aerodynamics of insect flight. J Exp Biol 206:4191–4208. doi:10.1242/jeb.00663

Spedding GR (1986) The wake of a jackdaw (*Corvus Monedula*) in slow flight. J Exp Biol 125:287–307

Spedding GR (1987) The wake of a kestrel (Falco Tinnunculus) in flapping flight. J Exp Biol 127:59–78

Spedding GR, Rayner JMV, Pennycuick CJ (1984) Momentum and energy in the wake of a pigeon (Columba Livia) in slow flight. J Exp Biol 111:81–102

Spedding GR, Rosen M, Hedenström A (2003) A family of vortex wakes generated by a thrush nightingale in free flight in a wind tunnel over its entire natural range of flight speeds. J Exp Biol 206:2313–2344. doi:10.1242/jeb.00423

Swartz SM, Groves MS, Kim HD, Walsh WR (1996) Mechanical properties of bat wing membrane skin. J Zool 239:357–378

Swartz SM, Bishop KL, Ismael-Aguirre M-F (2006) Dynamic complexity of wing form in bats: implications for flight performance. In: Akbar Z, McCracken G, Kunz T (eds) Functional and evolutionary ecology of bats. Oxford University Press, Oxford

Tian X, Iriarte-Diaz J, Middleton K, Galvao R, Israeli E, Roemer A, Sullivan A, Song A, Swartz S, Breuer K (2006) Direct measurements of the kinematics and dynamics of bat flight. Bioinspir Biomim 1:10–18

Tobalske BW, Hedrick TL, Dial KP, Biewener AA (2003a) Comparative power curves in bird flight. Nature 421:363–366

Tobalske BW, Hedrick TL, Biewener AA (2003b) Wing kinematics of avian flight across speeds. J Avian Biol 34:177–184

Willis DJ, Israeli ER, Persson P-O, Drela M, Peraire J, Swartz SM, Breuer KS (2007) A computational framework for fluid structure interaction in biologically inspired flapping flight. In: AIAA applied aerodynamics meeting, vol 1, pp 38–59, American Institute of Aeronautics and Astronautics Inc, Miami, United States, Reston, VA 20191–4344, United States